Flexural strength and rotation capacity of welded I-section steel beams with longitudinally profiled flanges

Liu, Xiaoling; Wang, Yuanqing; Ban, Huiyong; Liu, Ming; Veljkovic, Milan; Bijlaard, Frans S.K.

DOI
10.1016/j.jcsr.2020.106255

Publication date
2020

Document Version
Final published version

Published in
Journal of Constructional Steel Research

Citation (APA)
Liu, X., Wang, Y., Ban, H., Liu, M., Veljkovic, M., & Bijlaard, F. S. K. (2020). Flexural strength and rotation capacity of welded I-section steel beams with longitudinally profiled flanges. *Journal of Constructional Steel Research*, *173*, 1-15. Article 106255. https://doi.org/10.1016/j.jcsr.2020.106255

Journal of Constructional Steel Research 173 (2020) 106255

Contents lists available at ScienceDirect

Journal of Constructional Steel Research

Flexural strength and rotation capacity of welded I-section steel beams with longitudinally profiled flanges

Xiaoling Liu [a], Yuanqing Wang [a], Huiyong Ban [a,*], Ming Liu [b], Milan Veljkovic [c], Frans S.K. Bijlaard [c]

[a] Department of Civil Engineering, Tsinghua University, Beijing, China
[b] Angang Steel Company Limited, Anshan, China
[c] Department of Engineering Structures, Delft University of Technology, Delft, the Netherlands

ARTICLE INFO

Article history:
Received 3 March 2020
Received in revised form 8 July 2020
Accepted 10 July 2020
Available online xxxx

Keywords:
Welded I-section steel beam
Longitudinally profiled steel plate
Rate of thickness change
Flexural strength
Rotation capacity

ABSTRACT

Application of longitudinally profiled (LP) steel plate in the flange of flexural members may provide a good solution to optimize their mechanical performance and to improve the efficiency of steel use, whilst existing design codes provide no design guidance or prediction methodology for such advanced beams in terms of flexural behaviour. To clarify their flexural strength and rotation capacity, tests on two full-scale welded I-section steel beams with longitudinally profiled flanges (LPB members) are carried out herein, as well as two traditional beams with uniform cross-section for comparison. All the specimens exhibit sufficient flexural strength and rotation capacity for seismic plastic design, and specifically, the LPB members possess even better performance in case of identical steel usage. Parametric analyses of 250 beams incorporating a wide range of flange slenderness and steel grades, are conducted by employing the validated nonlinear FE model to investigate the effects of rate of thickness change for the LP flanges. The results show that the effect is limited on the flexural strength but significant on rotation capacity. The existing design provisions for beams with uniform cross-section give generally conservative design results for the flexural strength of the LPB members, but limiting values of flange slenderness needs to be reduced. The research outcomes may provide an important basis for promoting the application of LP plates in flexural members.

1. Introduction

Steel structures have been increasingly applied in practice in recent decades and are playing a vital role in the fields of structural engineering. Accordingly, a large number of investigations have been conducted at levels of material properties, member behaviour as well as structural performance, aiming at economic and reasonable structure design. But there is one apparent paradox that the cross-section of a single structural member is generally uniform and is determined based on the requirement of critical section, whilst distribution of internal force along the member length is usually nonuniform. Thus, optimisation in terms of geometry of cross-section is a natural and efficient solution to solve this problem. There have been some specific ways applied in practice for this optimisation, such as the use of tapered members with web height varying along the length in portal frames [1]. Besides, sometimes large span girders are designed with several segments and each segment has different cross-sectional height or flange thickness [2]. In recent years, the development of longitudinally profiled (LP) steel plate makes another new solution possible in terms of variable cross-sections.

LP steel plate is a kind of advanced structural steel product, of which thickness is varying continuously along its longitudinal direction. Commencing in 1983 when the first LP steel plate with a single wedge was produced in France [3], more other profiled shapes are now developed, as shown in Fig. 1 [4]. As a result, an optimised matching between geometry of steel plates and distribution of internal forces within structural members becomes possible. In practice, the LP steel plates have been used in several road and highway bridges [2], as well as shipbuilding construction [5], which is beneficial for reducing steel weight and welding amount [6].

It seems that the earliest studies are that focusing on the material properties of the LP steel plate reported by the French Highways Department [3] in the 1980s and steel mill maker NKK in Japan [6] in the 1990s. The tensile coupon test results showed their strength decreased generally with an increase of the thickness in a single steel plate, which is attributed to the different rolling temperatures and rolling compression ratios [6]. Fukumoto et al. [6] also pointed out that the strength difference could be reduced by improving rolling control technique and heat treatment, and be eventually ignored in practical design. Regarding

* Corresponding author.
E-mail addresses: liuxiaoling950718@163.com (X. Liu), wang-yq@tsinghua.edu.cn (Y. Wang), banhy@tsinghua.edu.cn (H. Ban), 13898006025@163.com (M. Liu), m.veljkovic@tudelft.nl (M. Veljkovic), f.s.k.bijlaard@tudelft.nl (F.S.K. Bijlaard).

https://doi.org/10.1016/j.jcsr.2020.106255
0143-974X/

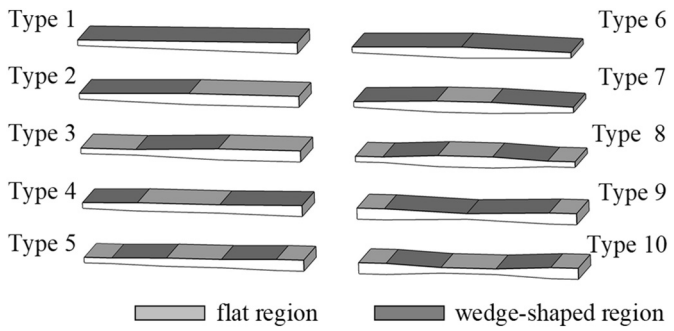

Fig. 1. Possible profile types of longitudinally profiled steel plates.

mechanical performance of structural members, Murakami and Nobuo [7] studied the ultimate strength of I-girders for bridges with tapered flange plates in 1997 based on the elasto-plastic finite element method. After that, more research focused on the hysteretic behaviour of square box piers fabricated with LP plates at the end, and extensive cycle loading tests were carried out to study the influence of the thickness change rate and length of the LP plates [8–11]. However, there is surprisingly limited research on the fundamental static behaviour of flexural members.

For simply supported I-section steel beams with LP flanges (referred to LPB members herein), the authors [12] previously investigated their deformation behaviour at the serviceability limit state and proposed a simplified design formula for predicting elastic deflection based on theoretical derivation. In the present paper, further research at the level of the ultimate limit state, including the flexural strength and rotation capacity, was concentrated on through experimental and numerical methodologies. Three and four-point loading scenarios were incorporated and different types of LP steel plates were employed following the specific distribution pattern of bending moment along the beam length. A three-dimensional finite element (FE) model was subsequently developed by using software ANSYS and validated against the test results obtained herein as well as against independent ones reported elsewhere. An extensive range of parametric analyses was carried out to clarify the effects of slenderness ratio of the LP flange plate, rate of the flange thickness change, and steel grades on their member performance. Comparisons with design results based on existing design standards were conducted, and design guidance was proposed for the LPB members.

2. Experimental investigation

2.1. Material properties

The LP steel plates used for fabricating the test specimens were manufactured by steelmaker Ansteel in China, including a single wedge LP plate labelled as SLP (corresponding to type 1 as shown in Fig. 1) with thickness varying from 12 mm to 46 mm and a nominal rate of thickness change being 6 mm/m, and a trapezoidal LP plate labelled as DLP (corresponding to type 7 as shown in Fig. 1) with an identical rate of thickness change but the thickness varying from 12 mm to 24 mm. Conventional steel plates with a uniform thickness of 12 mm and 24 mm, labelled as NP12 and NP24, respectively, were employed for comparison. Standard tensile coupon tests were conducted according to GB/T228.1–2010 [13] and GB/T 2975–2018 [14]. The tensile coupons were prepared from the LP plates as shown in Fig. 2(a) and (b) at locations with different nominal thicknesses, as well as from the NP plates.

All the tensile coupon tests were conducted by using a 1000kN testing machine at Tsinghua University. Two strain gauges were attached to the mid-length of the coupons, as shown in Fig. 2(c), to measure longitudinal strain at the elastic stage. An extensometer was also attached to get the strain at the elastoplastic stage. Characteristics of the stress-strain curves of the LP steel plate are similar to that of corresponding grades of conventional steel plates, as shown in Fig. 3.

Specific tensile coupon test results are summarised in Table 1 in terms of average values of the parallel coupons, where E is the Young's modulus, f_y denotes the nominal yielding strength (i.e. lower yield point), ε_{st} represents the strain at the onset of the strain hardening, f_u is the ultimate tensile strength, ε_u means the ultimate strain corresponding to f_u, and A is the elongation percentage after fracture. The test results show that the strength in a single LP plate decreases generally with an increase in the thickness of the plate, which nevertheless satisfies with requirements of Q420GJ steel grade, as shown in Fig. 4.

Regarding the coefficient of variation for the strengths, all of the data except for the yield strength variation of SLP were lower than the recommended upper limit 0.066 for conventional steel plates [15]. It implied relatively stable strength within a single LP plate. In manufacturing practice, it becomes more difficult to control the variation of strength in case of large variation in thickness within a single LP steel plate.

2.2. Design of beam specimens

A total of four full-scaled welded I-section beams, as shown in Fig. 5 (a), were tested under static loading. Two LPB members labelled as LPBS and LPBD, were subjected to 3-point loading and 4-point loading, respectively. These two loading conditions are selected as typical cases to study the flexural performance under moment gradient and uniform moment, which is a typical loading case for flexural member; for instance, simply-supported secondary beams, or the main girder of multi-story frame under earthquake load. Another two beams fabricated from conventional steel plate (referred to as NPB members here) were labelled NPBS and NPBD, respectively, for comparison. The most important parameter considered in this test was the type of the flange plate. Flanges of member LPBS were manufactured by welding 2 pieces of SLP together symmetrically because of no available double wedge steel plate (type6 shown in Fig. 1) in the market at the time. Flanges of member LPBD were prepared from plate DLP as needed, and all flanges of NPB members were prepared from plate NP24. The web of all the specimens was fabricated with the plate NP12. Transverse stiffeners were arranged at the corresponding position of loading and supporting sections by using the same plate as the web. The flanges and web were joined together by longitudinal fillet welds with a weld size h_f of 10 mm.

Fig. 5 also shows notations of longitudinal and sectional dimensions. The overall length l_0 for all beams was designed as being 6000 mm including span length l and 200 mm long overhanging segment at each end. The shear span is the range where flange thickness changed, and its length l_s of beams under 3-point loading was designed as being 2800 mm, and that of beams under 4-point loading was 1800 mm. The mid-span section had the maximum flange thickness t_f and the support end section was corresponding to the minimum thickness t_{f0}. As a result, in this paper, the rate α of thickness change of LP flanges was defined as a ratio of the flange thickness difference to the length of shear span, determined by $\alpha = (t_f - t_{f0})/l_s$. Dimensions of the beam specimens were measured and listed in Table 2 together with the amount of steel usage. Specimen LPBS had the same steel usage with specimen NPBS but its flange thickness was 1.36 times of that of the latter one at the critical section. Regarding specimens under 4-point loading, identical flange thickness at the mid-span was employed, and specimen LPBD saved 9.5% in terms of steel use compared with specimen NPBD.

The yielding moment M_y and plastic moment M_p, given as the product of the measured material properties and geometry, are shown in Table 3. Mid-span deflection Δ_p, as well as beam end rotation θ_p,

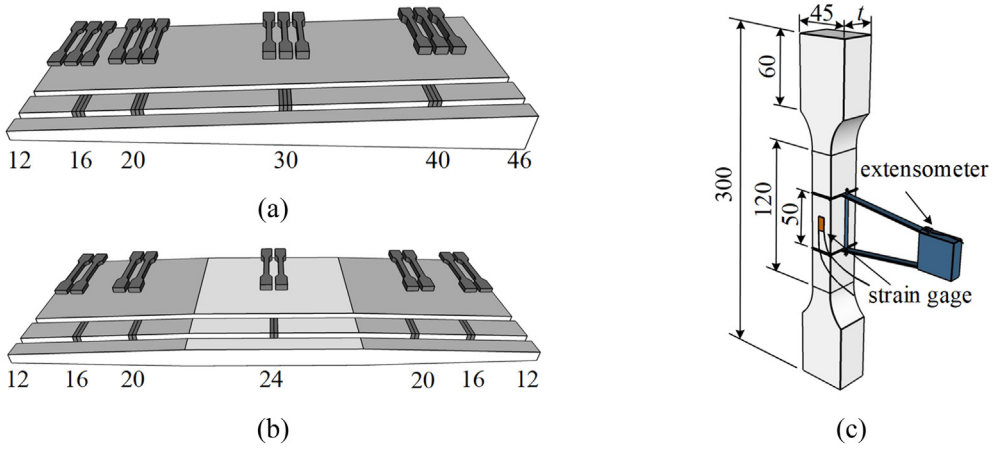

Fig. 2. Location of tensile coupons and test setup (unit: mm). (a) SLP; (b) DLP; (c) tensile coupon test setup.

which is the elastic component of deformation corresponding to M_p, was calculated considering the effect of flange thickness change of LPB members [12]. The mid-span deflection Δ_p was obtained using the theoretical solution presented in eq. (5b) and (6a) in [12], and the beam end rotation θ_p could be obtained based on the same method mentioned in Part 2 in [12]. The yield strength f_{yf} of flange at mid-span cross section and corresponding parameter f_{yf0} at support section, as well as the yield strength of web f_{yw}, were obtained by linear interpolation based on the experimental results for some certain values of thickness given in Table 1.

In terms of the specimen design, design provisions for NPB members were employed. The critical section was designed in accordance with S1 class (the most compact one) in GB50017–2017 [19], as well as sufficient lateral bracing was considered herein for the formation and full rotation of the expected plastic hinge. The class "S1" corresponds to the "Class 1" in Eurocode 3 [16] and "Seismic Compact(SC)" in ANSI/AISC 341–16 [18] from the prospect of desired performance, even if there are slight differences in the definition and limit values as shown in Table 4. Due to the change in flange thickness, the flange width-to-thickness ratio of the LPB members was continuously increased from the mid-span to the support end, as shown in Table 3. The width-to-thickness ratio b_f/t_{f0} of the flange within the support section satisfied the requirement of the class S2 in GB50017–2017, whilst it remained the same class as the mid-span section according to the other two national standards. The width-to-thickness ratio of the web varied little and always met the requirement of class S1.

2.3. Measurement of imperfections

The overall and local initial geometric imperfections were measured by using the methods reported in [20,21]. Measurement of initial geometric imperfections is illustrated in Fig. 6, which is determined by out-of-straightness at several cross-sections or reference points at the section. The measured results are listed in Table 5, all satisfying the requirements in accordance with GB 50205–2001 [22], in which the initial bending amplitude must be no more than L/1000 and 10 mm, the local defect value of flange must be no more than B/100 and 3 mm, and the local defect value of web must be no more than h_w/100.

2.4. Test setup and measurement

The beam tests were carried out by using loading equipment with a maximum bearing capacity of 5000 kN, as shown in Fig. 7. Two 1500 kN MTS hydraulic jacks with a maximum stroke of 250 mm were employed together to apply monotonic static loading. The beam specimen was simply-supported, with both ends being clamped to prevent torsion. Sufficient lateral restriction was provided by lateral bracing systems as illustrated in Fig. 7, so that the flexural-torsional buckling the beam specimens can be prevented, and the flexural strength and ductility can be focused on, which is the subject of the present research. During the loading process, load, strain, and displacement were recorded by using IMP data acquisition system. A preload with 5% to 10% theoretically estimated loading capacity was applied to eliminate the gap between test

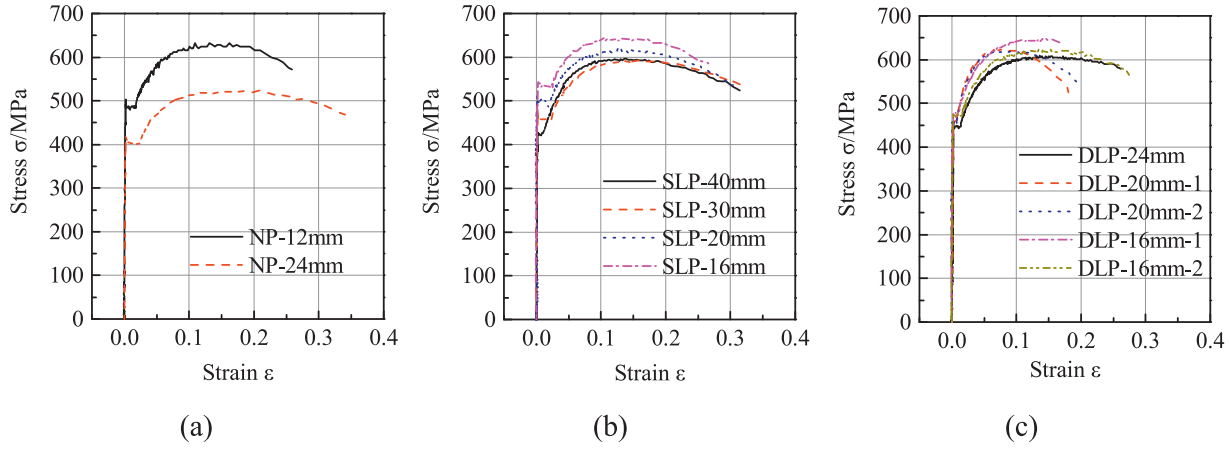

Fig. 3. Stress-strain curves. (a) NP12 and NP24; (b) SLP; (c) DLP.

Table 1
Tensile coupon test results.

Plate label	Thickness (mm)	Number of parallel coupons	E (MPa)	f_y (MPa)	ε_{st} (%)	f_u (MPa)	ε_u (%)	A (%)
NP12 (for webs)	12	3	205,495	489	1.77	636	13.42	28.33
NP24 (for flanges of NPB members)	24	3	207,885	405	2.53	526	18.09	29.53
SLP (for flanges of member LPBS)	16	3	209,950	543	2.39	653	12.63	25.02
	20	3	204,750	502	2.38	621	13.05	26.11
	30	3	208,970	464	2.30	601	15.46	28.09
	40	3	205,905	417	0.81	591	15.75	29.59
DLP (for flanges of member LPBD)	16	2	205,610	473	0.65	646	15.20	25.59
	20	2	205,045	455	0.72	619	9.02	28.29
	24	2	194,790	444	0.97	609	13.57	28.86
	20	2	203,810	459	0.78	623	8.14	29.92
	16	2	208,420	471	1.65	621	15.05	26.73

setup and the specimen, as well as to check the instrumentations and IMP system. The loading process was controlled by mid-span displacement and stopped in case of visible local buckling or load declining.

Layout of measurement is shown in Fig. 8, including that of linear variable displacement transducers (LVDTs) and strain gauges. For specimens under 3-point loading, 11 LVDTs were employed and labelled as D1 to D11. D1 to D3 were used to measure vertical displacement at the mid-span, 1/4 span, and 3/4 span, respectively. D6 and D9 were used to measure rigid body displacement at the supports. D4 and D5, as well as D7 and D8, were used to obtain the beam end rotation. Horizontal LVDTs D10 and D11 were placed near the end of lateral bracing beams to check the efficiency of the lateral support. A total of 58 strain gauges were attached on several cross-sections, among which sections 1 and 2 were 150 mm away from the mid-span where the plastic hinge was supposed to be formed; section 7 was 150 mm away from the supports, and sections 2 to 7 were evenly spaced to measure the strain distribution within cross-section with varying flange thickness. Layout of the strain gauges on the sections is shown in Fig. 8(c). For specimens under 4-point loading, layout of measurement was similar to that of beams under 3-point loading, and the only difference was that D2 and D3 were located at loading points. A total of 54 strain gauges were attached on six sections as shown in Fig. 8(b) and (c).

2.5. Test results and analyses

Fig. 9 shows moment versus beam end rotation response, in which the moment was normalised by the plastic moment resistance M_p, and the rotation was normalised by the plastic one θ_p. It can be seen that the bending moment increased gradually even beyond the plastic one M_p. When the vertical displacement at the loading point reached to the maximum stroke of hydraulic jacks, all the loading process was stopped. As a consequence, all the test curves did not show significant descending trend. Generally, slope of the load decreasing represents influence of local buckling, and smaller plate thickness results in lower descending rate [23]. Due to the small flange width-to-thickness ratio of the test specimens in this paper, the compression flanges were still effective even with significant local buckling being observed at the end of loading process.

Nevertheless, the whole moment versus rotation response curves were obtained by using the finite element (FE) method, and comparisons with the test results are given in the following section 3.2. Based on the validated FE results, the application of the LP steel plate in flanges of LPBS increased the member resistance by about 7.5% under the consumption of the same amount of steel. And about 9.5% of steel saved on LPBD when the performance was close.

All the four beam specimens failed by local buckling of the top compression flange, as shown in Fig. 10. For specimen LPBS, the compression flange near the loading point buckled locally, and the tensile flange at the mid-span cracked in the butt welded connection between two SLP steel plates at the end of loading. Specimens NPBS and LPBD exhibited more significant local buckling deformation within the shear span and next to the loading point compared with specimen LPBS; whilst for specimen NPBD, the local buckling occurred within the pure bending moment segment.

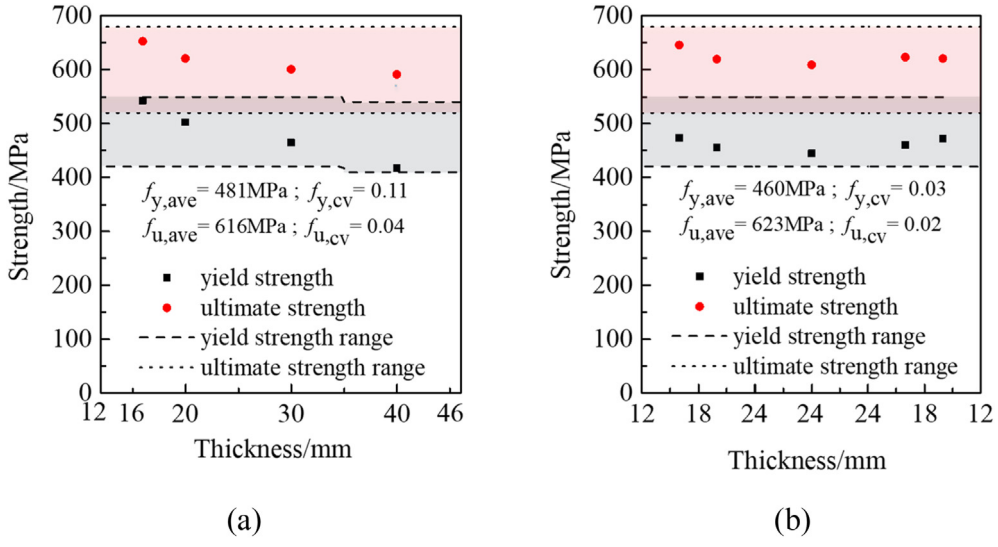

Fig. 4. Material strength change of LP steel plate along plate length. (a) SLP; (b) DLP.

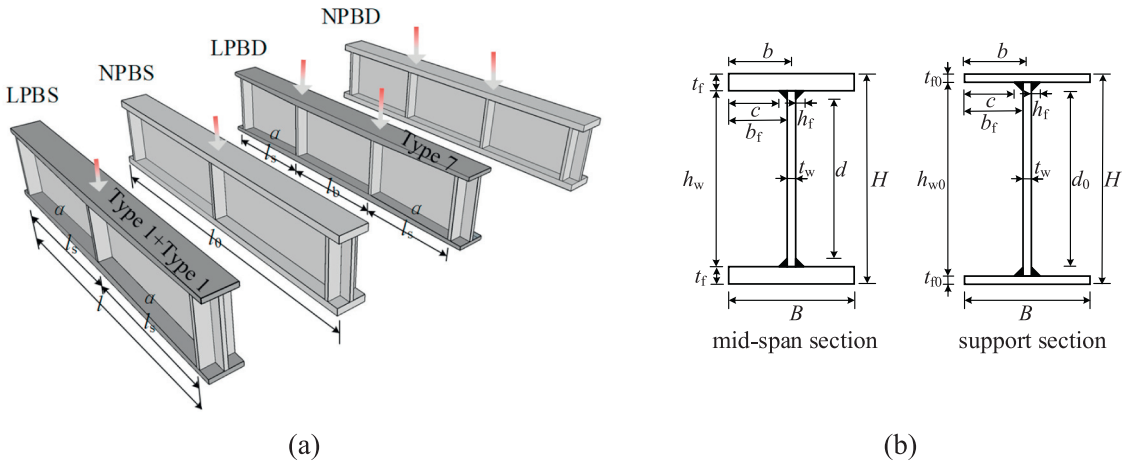

Fig. 5. Illustration of test specimens and dimensional symbols. (a) Illustration of test specimens; (b) Dimensional symbols of the section.

3. Finite element modelling and validation

In order to undertake extensive research with more parameters being involved on the beams with LP flanges, a three-dimensional FE model was developed, and further validated against independent beam tests, including that by Shi et al. [23], Shokouhian et al. [24], Lee et al. [25] and Green et al. [26], as well as against that introduced herein. It's worth noting that the four groups of independent beam tests were focusing on flexural and rotation capacity of I-section beams fabricated by conventional steel plate with various steel grades ranging from 345 MPa to 890 MPa.

3.1. FE modelling

FE models for simply support beams were developed by using software ANSYS with both material and geometric nonlinearities being incorporated. Multilinear isotropic hardening plasticity (MISO) material model with von Mises yielding rule was employed, and two types of multi-linear stress-strain relationship is utilized for material with or without visible yield plateau, respectively, as shown in Fig. 11. The parameters in the model was determined based on the uniaxial tensile coupon test results. The FE model was meshed with 4-node finite strain shell element SHELL181, which is commonly used for simulating flexural behaviour of beams [23,24] and has been proven adequate for analysis of thin-walled members. Given the minimum flange width-to-thickness ratio b_f/t_f of the specimens herein being less than 5, 8-node 3D solid element SOLID185 was also used for validation and comparison with the FE modelling results by using Shell181 elements. Mesh size was determined as around 15 to 25 mm through trial analyses with considerations of calculation efficiency and accuracy as well as convenience for sectional residual stress input. Initial imperfections including geometric ones and welding-induced residual stresses were taken into account in the FE model by using the method described in [20,21,27]. The lateral bracing system was simulated by constraining the lateral displacement of a row of nodes in the upper flange. Vertical displacement was applied at the loading point of FE models, and the Newton-Raphson Method was applied in analyses step. Typical FE model is shown in Fig. 12(a).

3.2. Validation of FE model against independent beam tests

Flexural behaviour of 39 beams reported elsewhere [23–26] was simulated by using the FE model developed herein, and comparisons of flexural strength between the FE modelling and test results are shown in Fig. 13. It was found that the average value (Ave) and standard deviation (SD) of the ratio between the FE analysis results by using element Shell181 to corresponding test results were 0.97 and 0.06, respectively; and they were 0.95 and 0.07, respectively in case of element Solid185 being utilized. The predictions from the FE model either using the shell element or solid element were in good agreement with the test results, and it is therefore confident to conclude that the FE model is adequate for simulating the behaviour of flexural beams.

3.3. Validation of FE model against dependent beam tests

Given the fact that there is no visible difference for predictions between FE models with shell and solid elements, element Solid185 was employed in the FE model to simulate the flexural behaviour of the beams tested herein, which is also favourable for accurately modelling variation of thickness for the LP steel plates. The LP flange was divided into 200 mm long segments because its material strength varied longitudinally, and each segment with different average thickness corresponded to different strengths that can be determined based on the tensile coupon test results (Table 1) by linear interpolation. Besides, the application of the LP steel plate not only caused the geometrical difference but also the shape of possible local imperfections, in this paper, the first order eigenvalue buckling mode was used.

Table 2
Measured dimensions and steel usage of beam specimens.

Beam label	Length			Flange				Web				Steel dosage (t)
	l_0 (mm)	l (mm)	l_s (mm)	B (mm)	t_f (mm)	t_{f0} (mm)	α (mm/m)	H (mm)	h_w (mm)	h_{w0} (mm)	t_w (mm)	
LPBS	6005.0	5599.5	2799.8	202.5	32.0	15.5	5.89	500.3	469.0	436.5	12.0	0.732
NPBS	6002.0	5601.0	2800.5	201.5	23.5		0	497.0	450.0		12.0	0.732
LPBD	5997.5	5600.5	1799.5	201.5	23.5	13.0	5.83	505.3	477.0	460.5	12.0	0.669
NPBD	6000.5	5600.5	1800.0	201.5	23.5		0	501.5	454.5		12.0	0.740

Table 3
Theoretical resistance and plate slenderness based on measured yield strength and dimensions.

Beam label	f_{yf} (MPa)	f_{yf0} (MPa)	f_{yw} (MPa)	M_y (kNm)	M_p (kNm)	Δ_p (mm)	θ_p (rad)	$(b_f/t_f)/\varepsilon_f^*$ ~$(b_f/t_{f0})/\varepsilon_{f0}^*$	$(h_w/t_w)/\varepsilon_w^*$ ~$(h_{w0}/t_w)/\varepsilon_w^*$
LPBS	455	543	489	1435	1660	29.55	0.017	4.14 ~ 9.34	36.38 ~ – 39.08
NPBS	405	405	489	1014	1205	24.56	0.013	5.29	37.50
LPBD	444	479	489	1050	1329	34.42	0.020	5.54 ~ 10.41	38.38 ~ 39.75
NPBD	405	405	489	1026	1220	31.50	0.018	5.29	37.88

* Coefficient $\varepsilon_f = (235/f_{yf})^{0.5}$, $\varepsilon_{f0} = (235/f_{yf0})^{0.5}$, $\varepsilon_w = (235/f_{yw})^{0.5}$.

Table 4
Maximum width-to-thickness ratios for compression parts of welded I-section beams.

Design code	Flange					web
Eurocode 3 [16]	Class 1	Class 2	Class 3		Class 4	Class 1
c/t_f	$\leq 9\varepsilon^*$	$\leq 10\varepsilon^*$	$\leq 14\varepsilon^*$		$>14\ \varepsilon^*$	$d/t_w \leq 72\varepsilon^*$
ANSI/AISC 360–16 [17]	Seismic compact [18]	Compact	Noncompact		Slender	Compact
b/t_f	$\leq 0.3(E^*/f_y)^{0.5} \approx 9\varepsilon^*$	$\leq 0.38(E^*/f_y)^{0.5} = 11\varepsilon^*$	$\leq 0.95(k_c E^*/f_l^*)^{0.5} \approx 26.5\varepsilon^*$		$>26.5\ \varepsilon^*$	$h_w/t_w \leq 110\varepsilon^*$
GB50017–2017 [19]	S1	S2	S3	S4	S5	S1
b_f/t_f	$\leq 9\varepsilon^*$	$\leq 11\varepsilon^*$	$\leq 13\varepsilon^*$	$\leq 15\varepsilon^*$	$\leq 20\varepsilon^*$	$h_w/t_w \leq 65\varepsilon^*$

* Coefficient $\varepsilon = (235/f_y)^{0.5}$; Elastic modulus $E = 200{,}000$; $0.35 \leq k_c = 4/(h_w/t_w)^{0.5} \leq 0.76$; $f_l = 0.7f_y$.

Moment-rotation curves obtained from the FE analyses with ideal lateral restriction bracing (LRB), i.e. direct lateral constraint, are plotted together with test results in Fig. 9. It can be found that the FE modelling curves are significantly lower than the test curves, and this is mainly because the friction between the specimen and the lateral bracing beam was not taken into account. As a result, the lateral bracing beams were also modelled in the updated FE model (i.e. that with actual LRB), as shown in Fig. 12(b), in which the contact interaction between the beam specimen and the support system was modelled by point-to-surface contact element, and the slip coefficient was taken as 0.5. As can be observed from Fig. 9, the updated FE model with actual LRB gave predictions agreeing much better with the test results. The FE modelling curves had higher peak moment capacity because of the earlier termination of the beam tests after the maximum stroke of jacks being reached. Difference between the predictions of the FE model and the test results may attribute to less efficiency of the boundary conditions provided by the test setup, as well as change of the material properties with variation of the thickness of the LP plates in the LPB members; nevertheless, the predictions of loading capacities are conservative. Generally, the FE model developed herein was demonstrated capable of simulating the flexural behaviour of beams with either LP flanges or conventional component plates.

4. Parametric analyses

To further clarify the effects of LP flanges on flexural behaviour of I-section beams with fully lateral restriction, an extensive range of parametrical analyses was conducted in this section. Trial analyses demonstrated that the strength variation along the length within the LP flange caused a slight difference in the performance at the elastoplastic

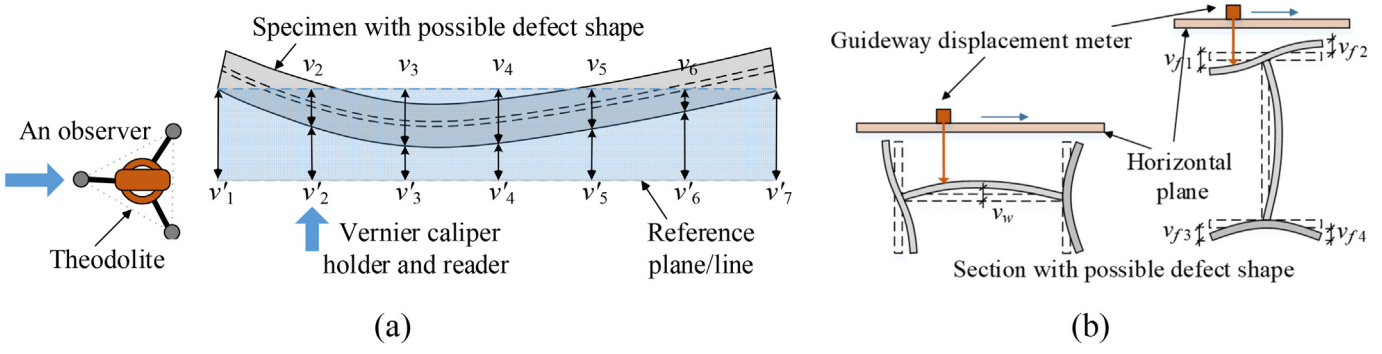

Fig. 6. Measurement of initial geometrical imperfections. (a) Illustration of overall geometrical imperfection measurement; (b) Illustration of local geometrical imperfection measurement.

Table 5
Measured geometric imperfection of beam specimens.

Beam label	Overall imperfections		Local imperfections	
	about minor axis direction	about major axis direction	flange	web
LPBS	l / 2042	l / 5089	B / 500	h_w / 297
NPBS	l / 1730	l / 1478	B / 396	h_w / 792
LPBD	l / 1964	l / 1817	B / 396	h_w / 305
NPBD	l / 1613	l / 3509	B / 524	h_w / 473

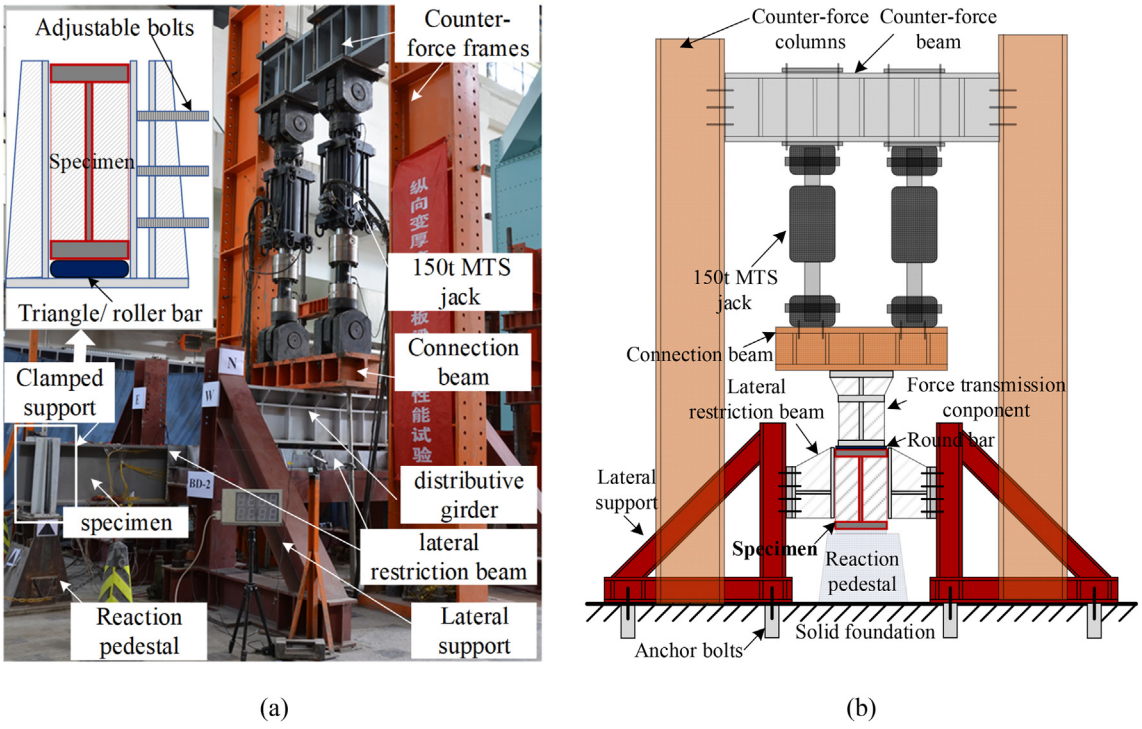

Fig. 7. Test setup. (a)Side view of setups and schematic diagram of clamped support; (b)Schematic diagram.

stage, thus a uniform material constitutive model was applied in subsequent parametric analyses.

4.1. Parameter range

A number of 25 LPBS members subjected to 3-point load with Q345 (345 MPa) steel, labelled as "LPBS-Q345", was designed as a control group, and a same control group was also designed for that under 4-point loading labelled as "LPBD-Q345". Parameter matrix of the standard group "LPBS-Q345" is given in Table 6. The beam designation stands for "LPBS - steel grade - flange width-to-thickness ratio b_f/t_f - rate of flange thickness change α". The other symbols in the table have the same meanings as mentioned before. For members of group "LPBD-Q345" subjected to 4-point loading, their parameters are identical to that of "LPBS-Q345", while the deformation should be recalculated according to [12].

Constant parameters included sectional height H of 500 mm, web thickness t_w of 12 mm, and maximum flange thickness t_f of 24 mm, as

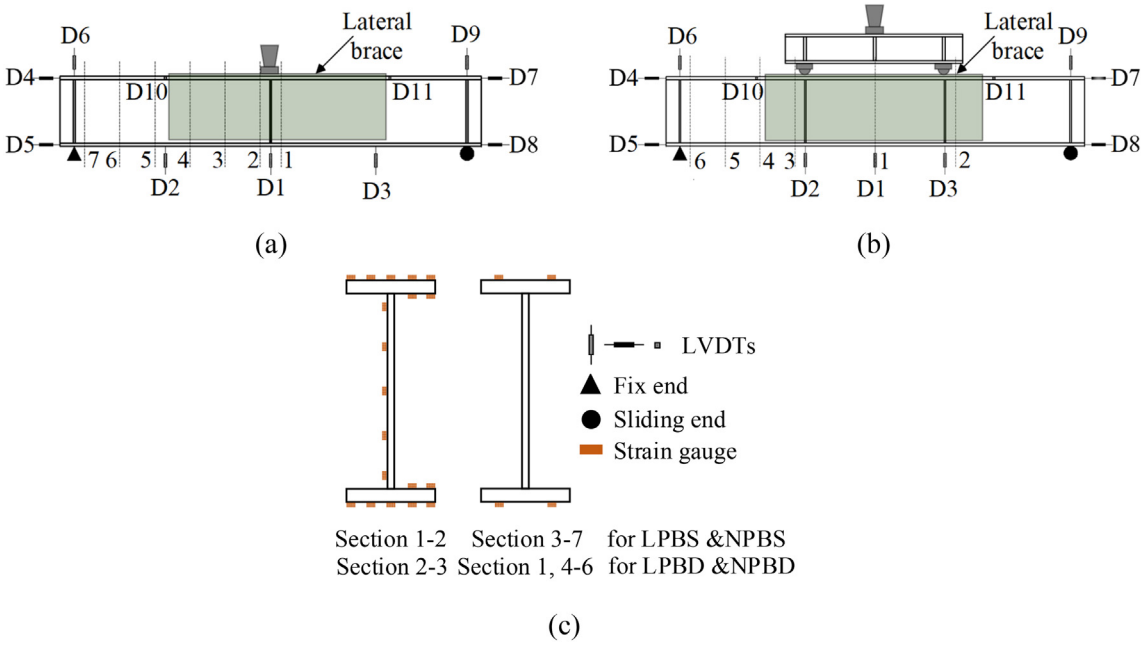

Fig. 8. Layout of measurement. (a) LPBS and NPBS; (b) LPBD and NPBD; (c) Strain gauge layout on cross-sections.

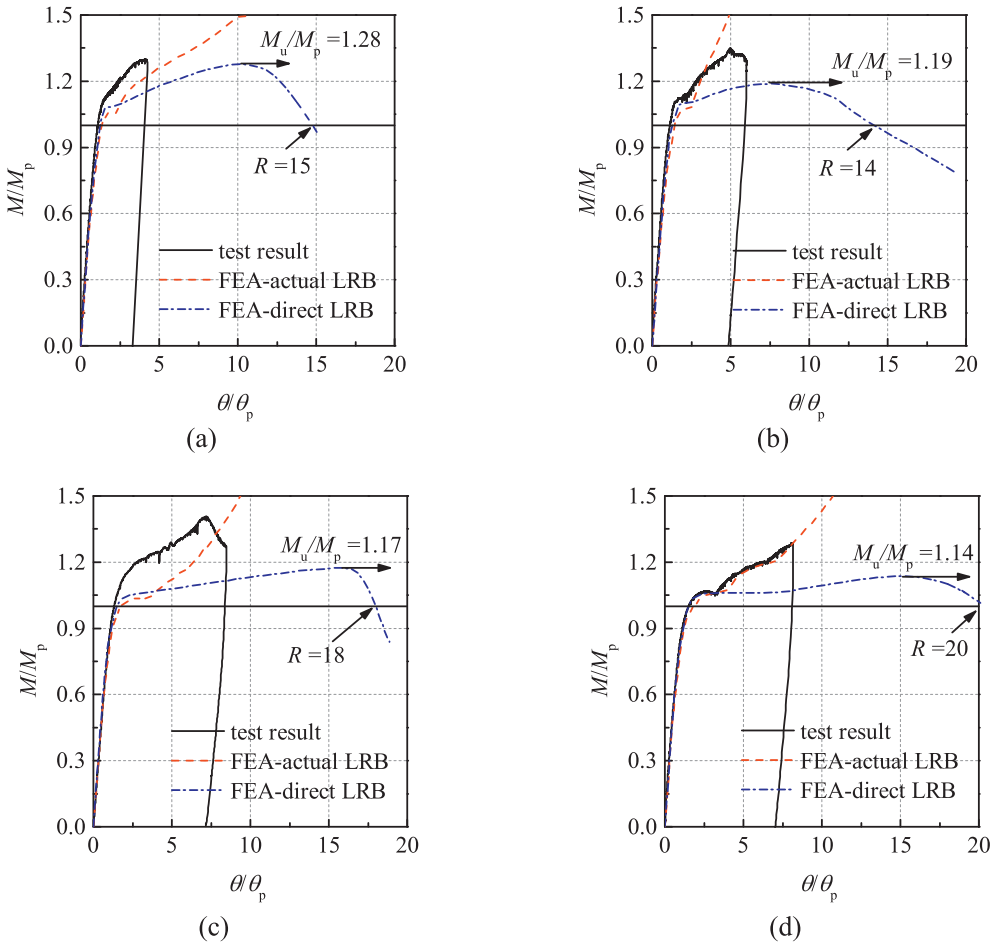

Fig. 9. Moment versus beam end rotation response from test results and FE analyses. (a)LPBS; (b)NPBS; (c)LPBD; (d)NPBD.

well as beam span l and shear span l_α. The length of all beams in group "LPBS-Q345" was 4 m ($l = 4$ m) with a shear span of 2 m ($l_\alpha = 2$ m), and beams in group "LPBD-Q345" were 6 m long ($l = 6$ m) with a shear span of 2 m long ($l_\alpha = 2$ m). Stiffeners were applied at the position of load points and support points. Compression flanges were restrained laterally.

Geometric parameters considered as variables herein mainly included width-to-thickness ratio b_f/t_f of flange and rate α of flange thickness change. Value of b_f/t_f ranged from 4 to 12 by changing the cross-sectional width B from 200 to 600, as shown in Table 6. Referred to LP steel plate products available in the market, value of α ranged from 0 (i.e. conventional steel plate) to 8 mm/m by varying thickness of flange t_{f0} at the support end from 24 to 8 mm, as shown in Table 6. Fig. 14(a) illustrates the various change rates of LP flange thickness together with the theoretical one (solid line) that completely agrees with distribution of internal moment. It can be seen that higher rate of flange thickness change may make moment resistance closer to the internal moment, i.e. to more economical design solution in case of strength design. In addition, it can be also found in Fig. 14(a) that the mid-span section remains the critical one for strength design.

Change of flange thickness may result in not only variation of sectional moment resistance along the beam length, but also variation of flange slenderness and thus the flange plate in one single beam may be classified differently. Taking the beam with a change rate of 8 mm/m for the LP flange for instance, its flange slenderness $\lambda_{f\alpha}$ changes with the thickness $t_{f\alpha}$, as shown in Fig. 14(b); it can be seen that values of $\lambda_{f\alpha}$ cover several classes according to the limiting values from national standards that are illustrated as horizontal lines in Fig. 14(b).

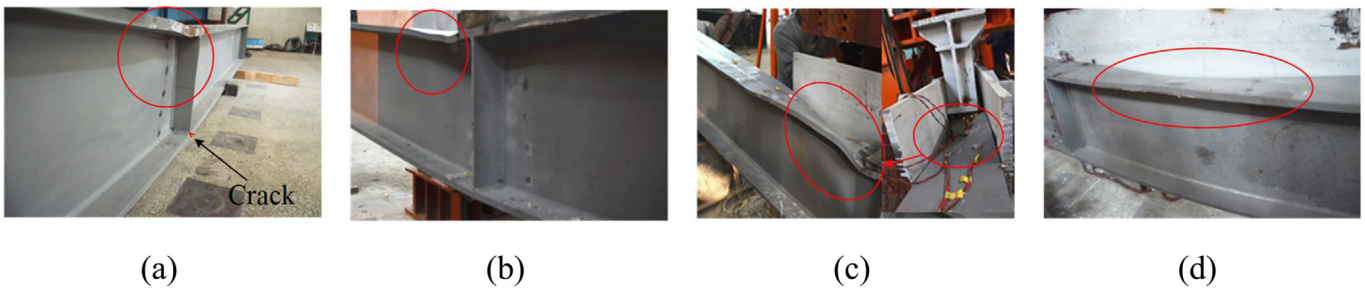

Fig. 10. Failure modes. (a) LPBS; (b)NPBS; (c)LPBD; (d)NPBD.

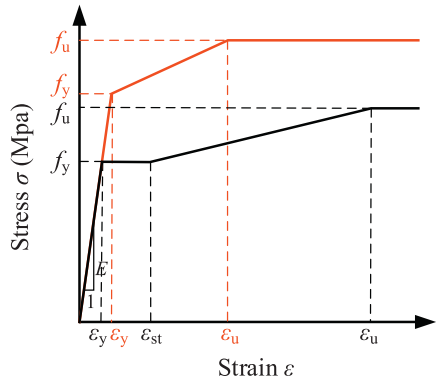

Fig. 11. Multi-linear material constitutive model for FE models.

The slenderness ratio of web varied slightly and satisfied with the requirement of plastic design.

In order to check the applicability of existing design provisions on the LPB members, design values of bending moment resistance M_d calculated by using the mid-span cross-section classification and material properties in accordance with Eurocode 3 [16], ANSI/AISC 360–16 [17], and GB50017–2017 [19] are summarised in Table 7. It should be noted that for calculating the design results from GB50017–2017, steel yield strength value f_y was employed rather than the design value f ($f = f_y / \gamma_R$, and γ_R denotes resistance partial coefficient of steel) to be consistent with the other two standards.

Regarding the steel grades incorporated in the parametric analyses, in addition to the steel grade (Q345, i.e. 345 MPa) most commonly used in practice, four other grades including Q420, Q460, Q550, and Q690 were also considered. Their uni-axial stress-strain relations and basic parameters [28] used in the analysis are shown in Fig. 15.

4.2. Effects of flange width-to-thickness ratio

To clarify effect of flange width-to-thickness ratio b_f/t_f on the flexural performance, comparisons of the moment versus rotation curves between NPB members ($\alpha = 0$) and LPB members ($\alpha = 8$ mm/m) are plotted in Fig. 16. It can be found that both the moment resistance and deformation capacity decreased generally with an increase of the flange width-to-thickness ratio for the beams with either NP or LP flanges, this is because compact section generally implied higher moment resistance and deformation capacity [23]. Besides, the moment resistance of NPB members was slightly larger than that of LPB members, and deformation capacity of the former was also slightly higher. This is because the section at other locations rather than the mid-span for the beams with NP flange was a little bit more compact than that of the beams with LP flange.

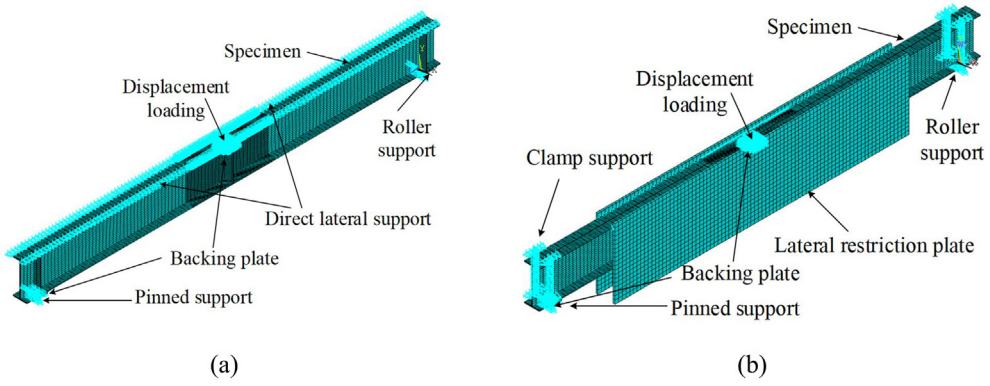

Fig. 12. FE model under 3-point loading. (a) FE model with direct lateral constraint; (b) FE model with actual lateral support.

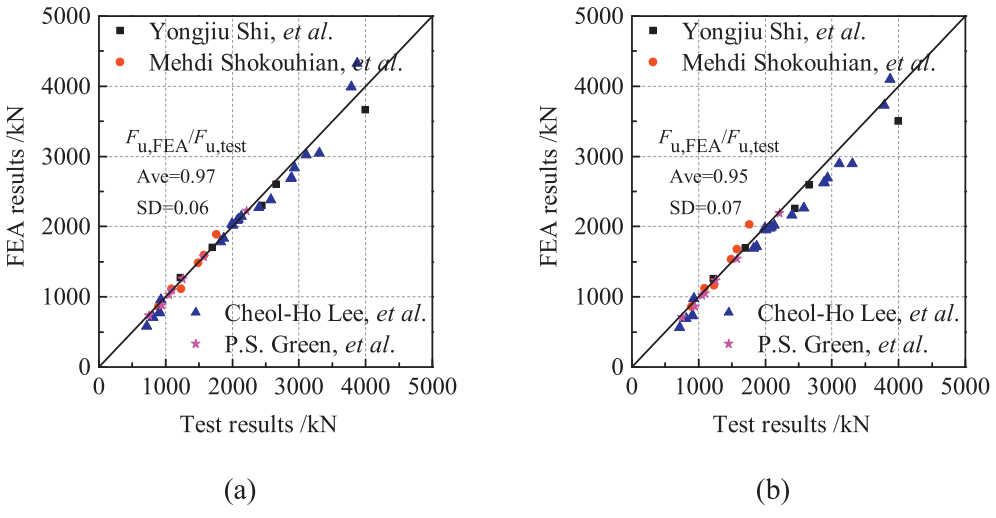

Fig. 13. Comparison of flexural strength between FE modelling and test results. (a) FE model with element Shell181; (b) FE model with element Solid185.

Table 6
Parameter matrix of beams in group LPBS-Q345.

No.	Beam designation	B (mm)	α (m/mm)	t_f (mm)	t_{f0} (mm)	b_f/t_f	b_f/t_{f0}	M_y (kNm)	M_p (kNm)	Δ_p (mm)	θ_p (rad)
1 ~ 5	LPBS-Q345-4-0,2,4,6,8	200	0 ~ 8	24	24 ~ 8	4	4 ~ 12	878	1000	10.16 ~ 11.77	0.008 ~ 0.009
6 ~ 10	LPBS-Q345-6-0,2,4,6,8	300	0 ~ 8	24	24 ~ 8	6	6 ~ 18	1254	1394	9.93 ~ 11.65	0.007 ~ 0.009
11 ~ 15	LPBS-Q345-8-0,2,4,6,8	400	0 ~ 8	24	24 ~ 8	8	8 ~ 24	1630	1788	9.80 ~ 11.59	0.007 ~ 0.009
16 ~ 20	LPBS-Q345-10-0,2,4,6,8	500	0 ~ 8	24	24 ~ 8	10	10 ~ 31	2005	2182	9.72 ~ 11.55	0.007 ~ 0.009
21 ~ 25	LPBS-Q345-12-0,2,4,6,8	600	0 ~ 8	24	24 ~ 8	12	12 ~ 37	2381	2576	9.67 ~ 11.52	0.007 ~ 0.009

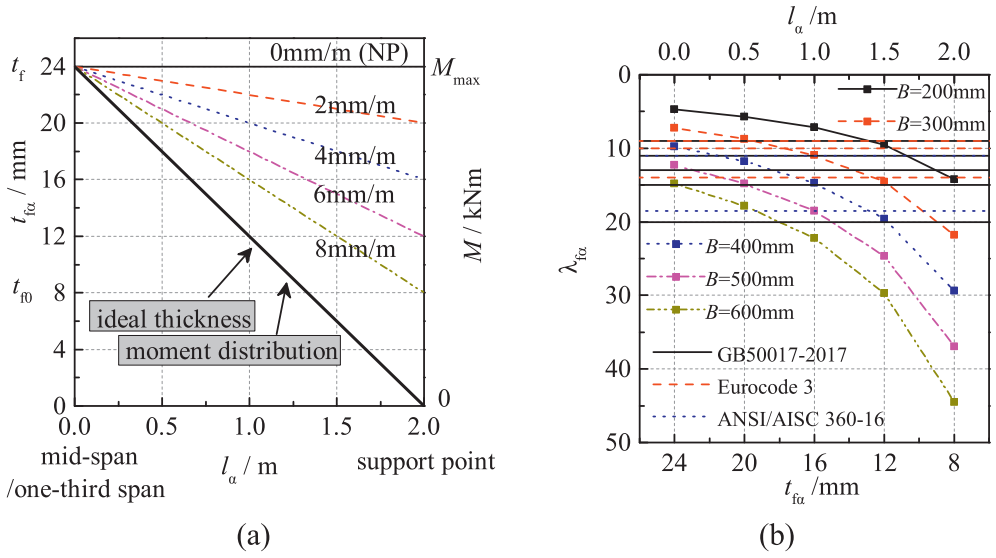

Fig. 14. Variation of flange thickness and slenderness along the shear span. (a) Flange thickness; (b) Flange slenderness.

Table 7
Flange plate classification and design moment resistance.

Beam designation	Eurocode 3 [16]		ANSI/AISC 360-16 [17]		GB50017-2017 [19]	
	Class	M_d(kNm)	Class	M_d(kNm)	Class	M_d(kNm)
LPBS-Q345-4-0 ~ 8	Cass 1 ~ 3	1000	C* ~ NC*	1000	S1 ~ S4	922
LPBS-Q345-6-0 ~ 8	Cass 1 ~ 4	1394	C* ~ NC*	1394	S1 ~ > S5	1317
LPBS-Q345-8-0 ~ 8	Cass 2 ~ 4	1788	C* ~ NC*	1788	S2 ~ > S5	1711
LPBS-Q345-10-0 ~ 8	Cass 3 ~ 4	2005	NC* ~ S*	2044	S3 ~ > S5	2105
LPBS-Q345-12-0 ~ 8	Cass 4	2342	NC* ~ S*	2119	S4 ~ > S5	2381

* C is the abbreviation of Compact, NC is the abbreviation of Noncompact, S is the abbreviation of Slender.

4.3. Effects of rate of flange thickness change

To elucidate effect of rate α of flange thickness change, relations between normalised moment M/M_p and beam end rotation θ/θ_p for beams with an identical flange slenderness ratio of six but various change rates α are plotted in Fig. 17. It can be seen that different variations of the flange thickness have generally no effects on the flexural performance at the elastic stage. But after the bending moment M reached M_p, ascending rate of the curve became lower and the descending rate beyond the peak point became steeper with an increase of α. Therefore, the LPB members have relatively lower moment resistance and rotation capacity compared with the NPB members with identical cross-section at their mid-span. In addition, effects of the rate α of flange thickness change became less significant for the LPB members under 4-point loading scenario, and this is because they have constant cross-section geometry within the pure bending region which mainly affects the overall flexural behaviour.

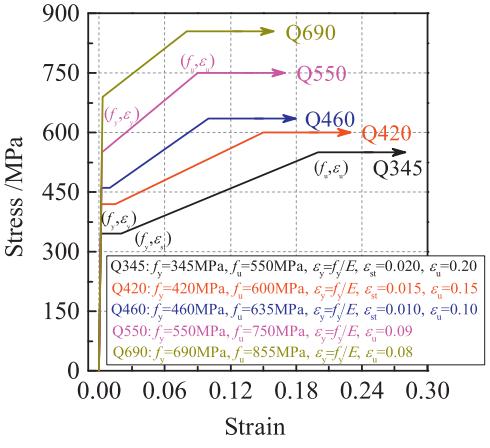

Fig. 15. Stress-strain relations of various steel grades.

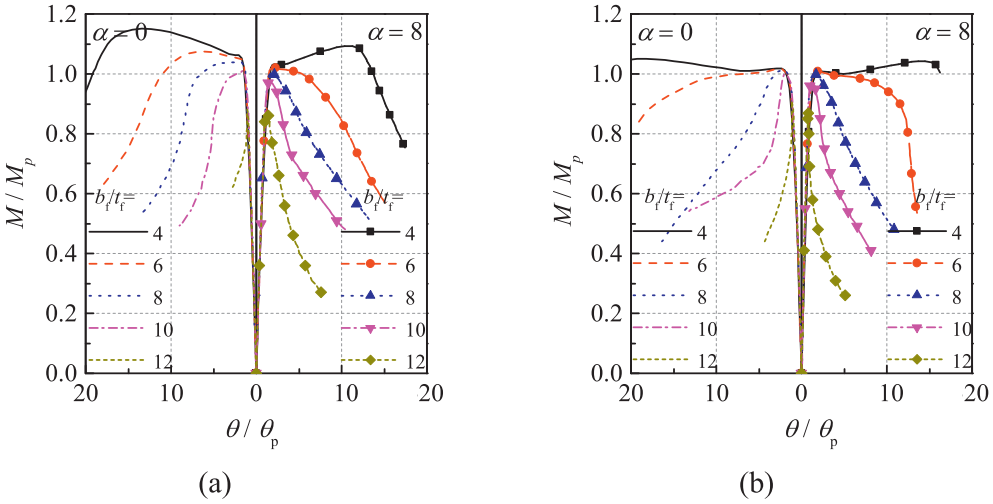

Fig. 16. Moment-rotation responses of beams with various flange width-to-thickness ratios. (a) LPBS-Q345; (b) LPBD-Q345.

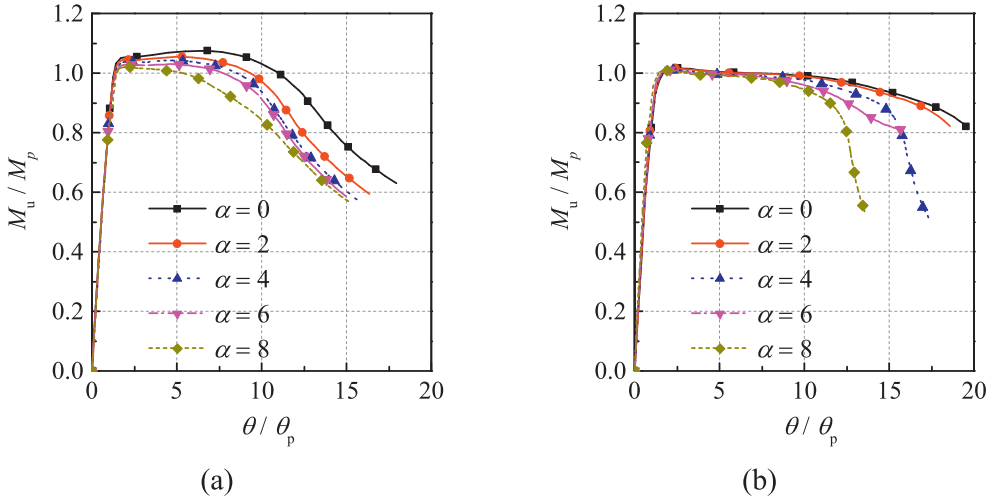

Fig. 17. Moment-rotation responses of beams with various rates of flange thickness change. (a) LPBS-Q345-6; (b) LPBD-Q345-6.

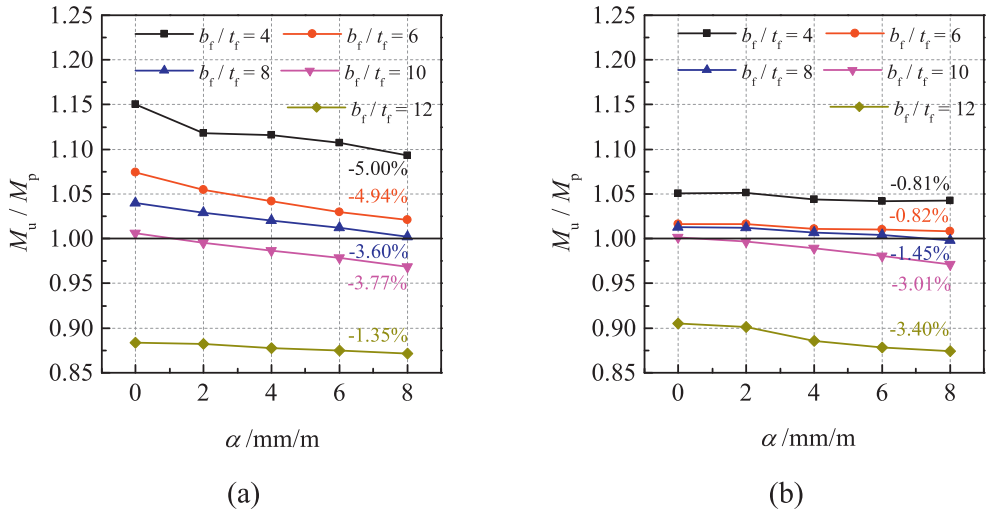

Fig. 18. Variation of the normalised ultimate moment with rate of flange thickness change. (a) LPBS-Q345; (b) LPBD-Q345.

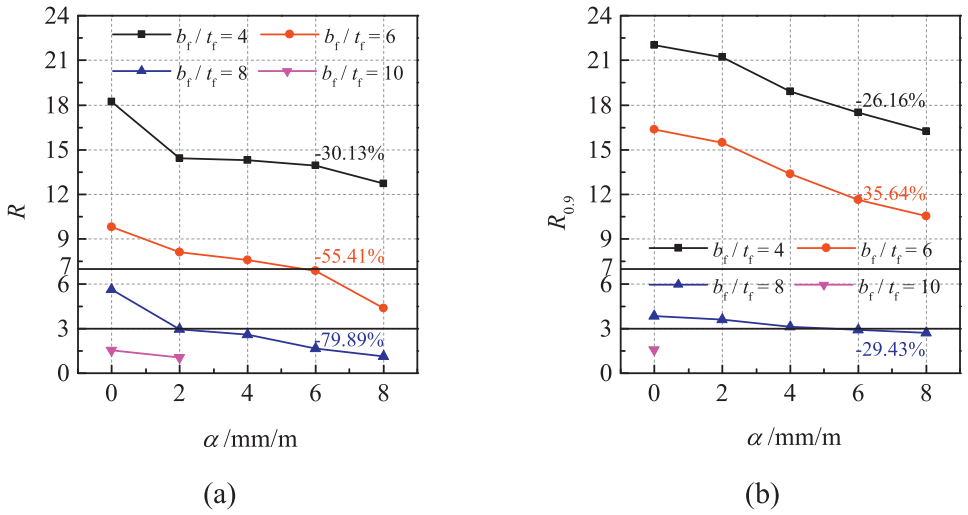

Fig. 19. Variation of the rotation capacity with rate of flange thickness change. (a) LPBS-Q345; (b) LPBD-Q345.

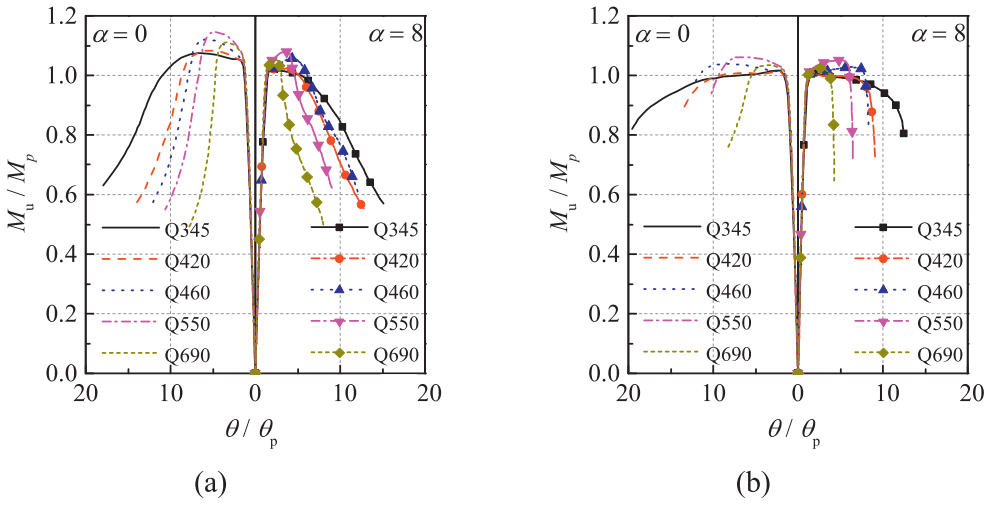

Fig. 20. Moment versus rotation responses of members with various steel grades. (a) LPBS; (b) LPBD.

To further quantify effects of the rate α of flange thickness change, the ultimate moment resistance M_u normalised by plastic moment M_p was obtained and is plotted in Fig. 18. It can be found that with an increase of α, the ultimate moment resistance of LPBS-Q345 members decreased by up to 5%, whilst it was 3.40% for LPBD-Q345 members. This indicated that the use of LP flange has generally negligible effects on the flexural strength of beams. Fig. 19 shows comparisons of rotation capacity R, which was defined herein for LPBS members as the difference between the beam end rotation θ_r corresponding to M_p in the descending part of curves and the rotation θ_p corresponding to plastic moment M_p in the ascending part, i.e. $R = \theta_r/\theta_p - 1$ [16]. For LPB members under 4-point loading, the rotation capacity $R_{0.9}$ was employed

Table 8
Cross section classification criteria for flexural members in national standards.

National standard	Cross section classification of flexural members				
Eurocode 3 [16]	Class 1	Class 2	Class 3		Class 4
	$M_u \geq M_p$	$M_u \geq M_p$	$M_p < M_u \leq M_y$		$M_u < M_y$
	R_s^* for plastic analysis	limited R_s^*	/		/
ANSI/AISC 360–16 [17]	Seismic compact [18]	Compact	Noncompact		Slender
	$M_u \geq M_p$	$M_u \geq M_p$	$M_p < M_u \leq 0.7M_y$		$M_u < 0.7M_y$
	R_s^* for plastic analysis	$R_s^* \geq 3$	/		/
GB50017–2017 [19]	S1	S2	S3	S4	S5
	$M_u \geq M_p$	$M_u \geq M_p$	$M_p > M_u > M_y$	$M_p > M_u \geq M_y$	$M_u < M_y$
	$\varphi^*/\varphi_p = 8 \sim 15$	$\varphi^*/\varphi_p = 2 \sim 3$	web partial plastic	no plastic	/

* φ represents the curvature of the section, R_s represents the rotation capacity of the section. For beam under uniform moment bending, $R_s = \varphi a$ (a denotes the length of uniform moment region, while for gradient moment bending, $R_s = \int \varphi dl$ (l denotes the length of plastic hinge region).

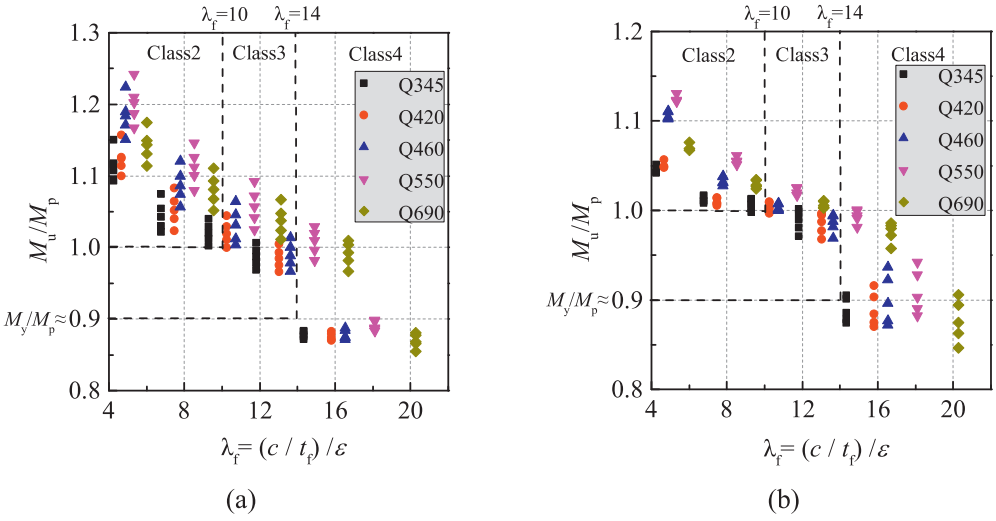

Fig. 21. Variation of normalised ultimate moment resistance with flange slenderness and comparisons with Eurocode 3. (a) LPBS; (b) LPBD.

($R_{0.9} = \theta_{r0.9}/\theta_p - 1$) in which $\theta_{r0.9}$ is corresponding to moment $0.9M_p$ in the descending part [24]. Based on Fig. 19, it can be seen that decrease of the rotation capacity R with an increase of the rate α of flange thickness change is more significant, especially for the LPBS members with a maximum reduction of up to 80%.

4.4. Effects of steel grades

Fig. 20 shows comparisons of moment versus rotation responses of beams with different steel grades, taking that with a flange width-to-thickness ratio of six for instance. It can be seen that for beams with compact sections and laterally braced compression flanges, their rotation capacity decreases with an increase of steel grade. This phenomenon can be attributed to the characteristic of stress-strain relationships for high-strength (HS) steels, including the yield strength, the yielding-to-tensile ratio, especially the yield platform, which is the determining factor of the simplified curvature distribution [25]. With respect to the ultimate moment resistance of beam, its absolute value gradually increased with an increase of the steel grades ranging from Q345 to Q550, while its normalised value M_u/M_p reduced dramatically from Q550 to Q690. This lower overstrength could be explained by the much higher yield strength used to calculated the plastic moment M_p, but the relatively small tensile strength f_u, which means that the M_u/M_p could be improved by reducing the yield ratio f_y/f_u [29].

5. Design guidance

Design of the flexural members could be classified into three categories, i.e., elastic, plastic, and seismic design according to the cross section classification. The requirements of flexural strength and rotation capacity under different classification are summarised in Table 8 in accordance with national standards. It can be seen that the relation of the cross section classification with moment resistance is pretty clear, but that with rotation capacity is not. The reason is that the requirement of rotation in plastic hinge depends on the type of the structure, e.g. continuous beam or frame [29], with the lowest value which is sufficient for forming the mechanism. A minimum rotation capacity of three is implied in the American national standard [17] for compact sections, while a value about 7 was suggested for seismic compact sections according to [25].

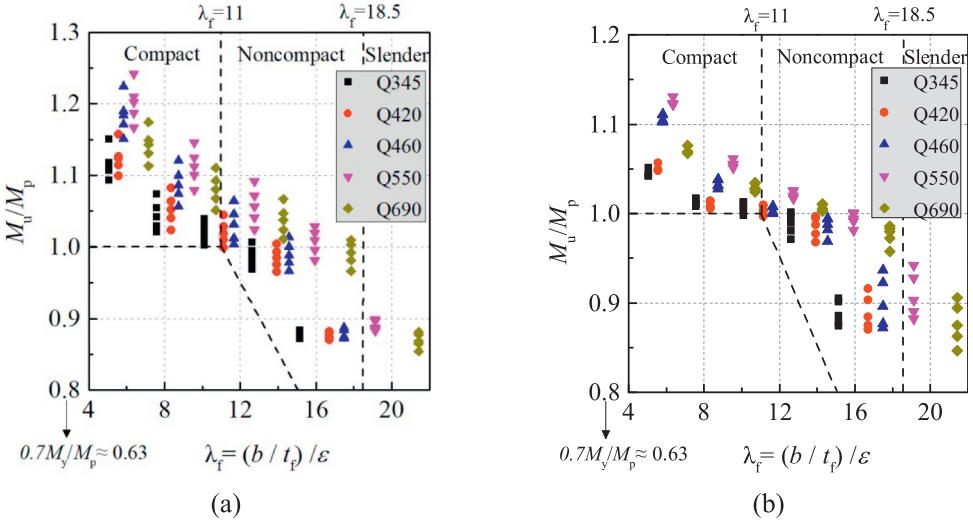

Fig. 22. Variation of normalised ultimate moment resistance with flange slenderness and comparisons with ANSI/AISC 360–16. (a) LPBS; (b) LPBD.

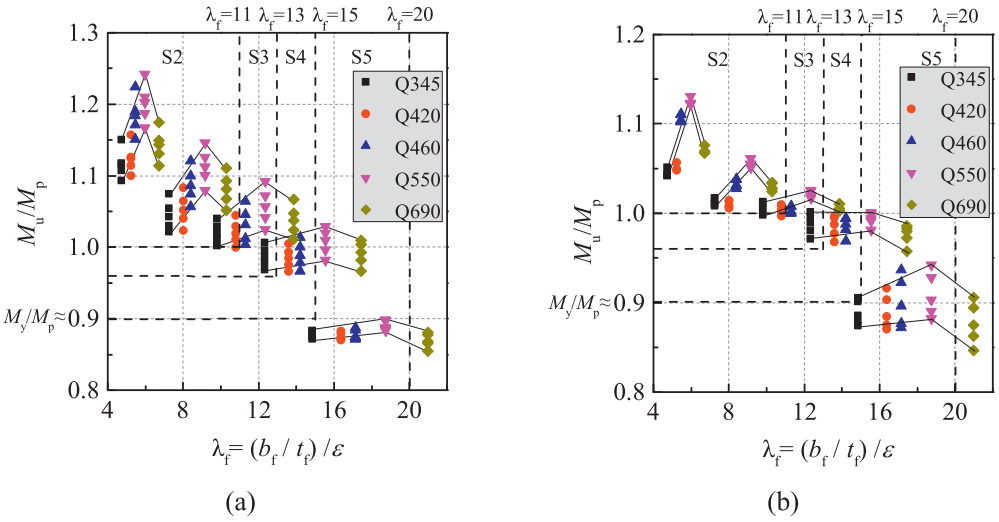

Fig. 23. Variation of normalised ultimate moment resistance with flange slenderness and comparisons with GB 50017–2017. (a) LPBS; (b) LPBD.

Comparisons of all the 250 parametric analysis results in terms of the flexural strength with design results in accordance with three national standards are shown in Fig. 21, Fig. 22, and Fig. 23, respectively. With respect to rotation capacity, comparisons with the available requirement of rotation capacity above are shown in Fig. 24. For each group of data points with identical plate slenderness ratio, the rate of thickness change increases from top to bottom.

As for the flexural strength M_u of LPB members whose flange slenderness at critical section is within the limits specified in three national standards for compact sections, it can be found that all the FE modelling predictions are higher than the boundary line M_p. When it comes to LPB members with much slender flanges at the critical section, most of the FE modelling results meet the requirements of the specification, but only flexural strength of LPB members labelled as "LPBS-Q345-12-0 ~ 8" and "LPBD-Q345-12-2 ~ 8" is slightly lower than that based on GB50017–2017 [19]. Nevertheless, it demonstrates that the flange slenderness limits given in national standard for classification are generally sufficient for the LPB members in terms of the flexural strength. As a consequence, the design methods for flexural strength of NPB members in current national standards are also applicable to LPB members with its critical cross-sectional property. Taking the Eurocode 3 [16] for example, the design bending resistance about one principal axis should be determined as follows:

$$M_d = \frac{W_{p,c} f_y}{\gamma_{M0}}, \text{for Class 1 or 2 cross sections} \quad (1)$$

$$M_d = \frac{W_{e,c} f_y}{\gamma_{M0}}, \text{for Class 3 cross sections} \quad (2)$$

$$M_d = \frac{W_{eff,c} f_y}{\gamma_{M0}}, \text{for Class 4 cross sections} \quad (3)$$

where $W_{p,c}$, $W_{e,c}$, $W_{eff,c}$ are the plastic section modulus, elastic section modulus and effective section modulus of the critical section, respectively.

As can be seen in Fig. 24, the rotation capacity R of all NPB members can meet requirement of 7 and 3, under the existing flange slenderness limit for seismic compact and compact sections in American standard (9 and 11, respectively). However, not all LPB members could obtain

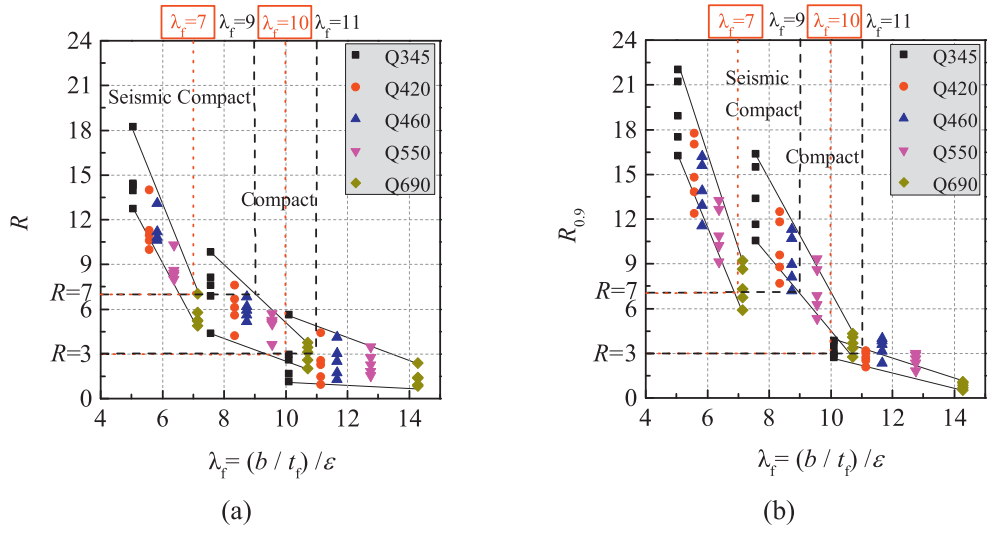

Fig. 24. Variation of the member ductility with flange slenderness and comparison with requirements in American national standard. (a) LPBS; (b) LPBD.

satisfactory results. More specifically, some LPB members whose critical section with a flange slenderness ratio between 7 and 9 cannot obtain rotation capacity larger than 7, as well as some with slenderness ratio between 10 and 11 cannot meet the requirement of 3. This is because of the adverse effect of the flange thickness change on ductility, and the existing slenderness limits are not sufficient when LP flanges are used. As a consequence, lower flange slenderness limits of 7 and 10 are obtained and suggested herein for the critical section of LPB members for seismic and plastic analysis, respectively. The modified slenderness limits are labelled in Fig. 24 and could cover all the predicted results.

6. Conclusions

To evaluate flexural strength and rotation capacity of welded I-section steel beams with LP flanges, two full-scaled beams subjected to 3-point and 4-point loading were tested, as well as the other two beams fabricated from conventional steel plates for comparison. A three-dimensional FE model was developed with variation of flange thickness and its material strength being accurately simulated. Based on validation against independent beam tests reported elsewhere as well dependent ones introduced herein, extensive parametric analyses on 250 beams were carried out to investigate effects of rate of flange thickness change, flange width-to-thickness ratio, and steel grades. Comparisons with design results in accordance with existing national standards were also conducted for proposing design guidance of beams with LP flanges. Based on the research findings, the following conclusions can be made:

1) Despite stress-strain curves of LP steel plate similar to that of corresponding ordinary steel plate, their material strength decreases with an increase of thickness within a single plate. However, this new feature of LP steel plate has slight effects on the elastoplastic behaviour of beams and therefore can be ignored in practical design.
2) LPB specimens designed in accordance with S1 class in GB50017–2017 may develop ultimate flexural strength beyond M_p as well as sufficient rotation capacity for seismic plastic design. Application of LP steel plate as flanges in beams increases their flexural strength by about 7.5% compared with beams with NP flanges that have same amount of steel use. Conversely, about 9.5% of steel may be saved by using LP flanges in beams compared with ordinary beams with similar flexural performance.
3) The use of LP steel plates as flanges in beams may not only lead to different geometry of cross sections but also to different shapes of potential local imperfections. As a result, degradation of flexural strength beyond the peak point as well as that of rotation capacity become more severe with an increasing rate of the LP flange thickness change. However, it was indicated that effect of LP flange on the ultimate flexural strength was rather limited.
4) Based on comparisons of parametric analysis results involving a wide range of rates of flange thickness change, flange width-to-thickness ratios, and steel grades with the design results in accordance with Eurocode 3, ANSI/AISC 360–16 and GB 50017–2017, it can be found that all three national standards may give conservative design results generally for flexural strength of LPB members with fully lateral restriction, but the lower limit of flange slenderness of 7 and 10 at critical section are suggested for seismic and plastic analysis ($R \geq 7$ and $R \geq 3$), respectively.

Declaration of Competing Interest

The authors declare that they have no known competing financial interests or personal relationships that could have appeared to influence the work reported in this paper.

Acknowledgments

The research work presented in this paper was financially supported by the National Key R&D Program of China (2018YFC0705503). The financial support provided by the China Scholarship Council (CSC) to the first author for her visit to TU delft is also acknowledged.

References

[1] G.Q. Li, J.J. Li, A tapered Timoshenko-Euler beam element for analysis of steel portal frames, J. Constr. Steel Res. 58 (12) (2002) 1531–1544.
[2] J. Brozzetti, Design development of steel-concrete composite bridges in France, J. Constr. Steel Res. 55 (1) (2000) 229–243.
[3] K. Richter, H. Schmackpfeffer, Longitudinally profiled plated cut costs, Join. Mater. 1 (6) (1988) 270–273.
[4] GB/T 37800–2019, Hot Rolled Longitudinally Profiled Steel Plate, Standards Press of China, Beijing, 2019 (in Chinese).
[5] S. Suzuki, R. Muraoka, T. Obinata, S. Endo, T. Horita, K. Omata, Steel products for shipbuilding, JFE Technical Report 2004, pp. 41–48 , vol. 2.
[6] Y. Fukumoto, M. Nagai, Steel bridges: new steels and innovative erection methods, Prog. Struct. Eng. Mater. 2 (2000) 34–40Y. Fukumoto, T. Takaku, T. Aoki, K.A.S. Susantha, Innovative use of profiled steel plates for seismic structural performance, Adv. Struct. Eng. 8 (3) (2005) 247–257.
[7] S. Murakami, N. Nobuo, Ultimate strength evaluation of tapered plate in compression, Proc. 5th International Colloquium on Stability and Ductility of Steel Structures, Nagoya 1997, pp. 133–140.
[8] Y. Fukumoto, M. Uenoya, M. Nakamura, H. Saya, Cyclic performance of stiffened square box columns with thickness tapered plates, Int. J. Steel Struct. 3 (2) (2003) 107–115.
[9] T. Takaku, Y. Fukumoto, T. Aoki, K.A.S. Susantha, Seismic design of bridge piers with stiffened box sections using LP plates, Proc. 13th World Conference on Earthquake Engineering, Vancouver, B.C 2004, pp. 3224–3239.
[10] K.A.S. Susantha, T. Aoki, T. Kumanob, Strength and ductility evaluation of steel bridge piers with linearly tapered plates, J. Constr. Steel Res. 62 (9) (2006) 906–916.
[11] T. Aoki, T. Takaku, Y. Fukumoto, K.S.A. Susantha, Experimental investigation for seismic performance of framed structures having longitudinally profiled plates, J. Constr. Steel Res. 64 (7) (2008) 875–881.
[12] Y.Q. Wang, X.L. Liu, H.Y. Ban, M. Liu, Y.J. Shi, Y.Y. Wang, Deformation behavior at SLS of welded I-section steel beams with longitudinally profiled flanges, J. Constr. Steel Res. 146 (2018) 122–134.
[13] GB/T 228.1-2010, Metallic Materials—Tensile Testing—Part 1: Method of Test at Room Temperatures, Standards Press of China, Beijing, 2011 (in Chinese).
[14] GB/T 2975–2018, Steel and Steel Products—Location and Preparation of Samples and Test Pieces for Mechanical Testing, Standards Press of China, Beijing, 2018 (in Chinese).
[15] G. Shi, X. Zhu, H. Ban, Material properties and partial factors for resistance of high-strength steels in China, J. Constr. Steel Res. 121 (2016) 65–79.
[16] BS EN 1993-1-1: 2005, Eurocode 3: Design of Steel Structures—Part 1–1: General Rules and Rules for Buildings, British Standards Institution, London, 2005.
[17] ANSI/AISC 360-16, Specification for Structural Steel Buildings, American Institute of Steel Construction, Chicago, 2016.
[18] ANSI/AISC 341-16, Seismic Provisions for Structural Steel Buildings, American Institute of Steel Construction, Chicago, 2016.
[19] GB 50017–2017, Standard for Design of Steel Structures, China Architecture & Building Press, Beijing, 2017 (in Chinese).
[20] H. Ban, G. Shi, Y. Shi, Y. Wang, Overall buckling behavior of 460MPa high strength steel columns: experimental investigation and design method, J. Constr. Steel Res. 74 (2012) 140–150.
[21] H.X. Yuan, Y.Q. Wang, L. Gardner, Y.J. Shi, Local-overall interactive buckling of welded stainless steel box section compression members, Eng. Struct. 67 (2014) 62–76.
[22] GB 50205–2001, Code for Acceptance of Construction Quality of Steel Structures. , Standards Press of China, Beijing, 2002 (in Chinese).
[23] Y.J. Shi, K.L. Xu, G. Shi, Y.X. Li, Local buckling behavior of high strength steel welded I-section flexural members under uniform moment, Adv. Struct. Eng. 21 (1) (2017) 93–108.
[24] M. Shokouhian, Y. Shi, Flexural strength of hybrid steel I-beams based on slenderness, Eng. Struct. 93 (2015) 114–128.
[25] C.H. Lee, K.H. Han, C.M. Uang, D.K. Kim, C.H. Park, J.H. Kim, Flexural strength and rotation capacity of I-shaped beams fabricated from 800-MPa steel, J. Struct. Eng. 139 (6) (2013) 1043–1058.
[26] P.S. Green, R. Sause, J.M. Ricles, Strength and ductility of HPS flexural members, J. Constr. Steel Res. 58 (2002) 907–941.
[27] H.Y. Ban, G. Shi, Overall buckling behaviour and design of high-strength steel welded section columns, J. Constr. Steel Res. 143 (2018) 180–195.
[28] GB/T 1591-2008, High Strength Low Alloy Structural Steels, Standards Press of China, Beijing, 2009 (in Chinese).
[29] M. Pavlovic, M. Veljkovic, Compact cross-sections of mild and high-strength steel hollow-section beams, Proceed. Institut. Civil Eng. Struct. Build. 170 (11) (2017) 825–840.